A Graphene-Based Sensor Array for High-Precision and Adaptive Target Identification with Ensemble Aptamers

Hao Pei,[†] Jiang Li,[†] Min Lv,[†] Jingyan Wang,[†] Jimin Gao,[‡] Jianxin Lu,[‡] Yongping Li,[†] Qing Huang,[†] Jun Hu,*[,†] and Chunhai Fan*[,†]

[†]Laboratory of Physical Biology, Shanghai Institute of Applied Physics, Chinese Academy of Sciences, Shanghai 201800, China
[‡]Key Laboratory of Laboratory Medicine, Ministry of Education, Wenzhou Medical College, Wenzhou 325035, Zhejiang, China

Ⓢ *Supporting Information*

ABSTRACT: In this work, we report a new concept of adaptive "ensemble aptamers" (ENSaptamers) that exploits the collective recognition abilities of a small set of rationally designed, nonspecific DNA sequences to identify molecular or cellular targets discriminatively. In contrast to in vitro-selected aptamers, which possess specific "lock-and-key" recognition, ENSaptamers rely on pattern recognition that mimics natural olfactory or gustatory systems. Nanographene oxide was employed to provide a low-background and highly reproducible fluorescent assay system. We demonstrate that this platform provides a highly discriminative and adaptive tool for high-precision identification of a wide range of targets for diagnostic and proteomic applications with a nearly unlimited supply of ENSaptamer receptors.
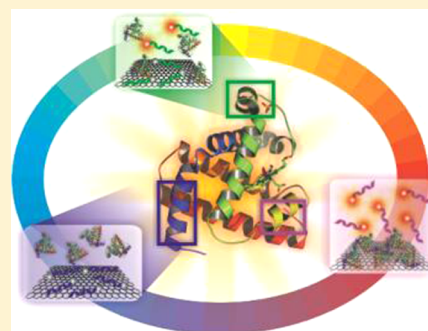
INTRODUCTION

There have been long-lasting efforts to discover natural and develop artificial receptors (e.g., antibodies and aptamers) for diverse applications, including medical diagnostics and therapeutics.[1−6] However, the limited supply of high-specificity receptors forms a major bottleneck for these purposes.[7,8] Here we report a new concept of adaptive "ensemble aptamers" (ENSaptamers) that exploits the collective recognition abilities of a small set of rationally designed, nonspecific DNA sequences to identify molecular or cellular targets discriminatively. In contrast to in vitro-selected aptamers, which possess specific "lock-and-key" recognition, ENSaptamers rely on pattern recognition that mimics natural olfactory or gustatory systems.[9] Nanographene oxide (NGO) was employed to provide a low-background and highly reproducible fluorescent assay system.[10−12] We demonstrate that this platform provides a highly discriminative and adaptive tool for high-precision identification of a wide range of targets for diagnostic and proteomic applications with a nearly unlimited supply of ENSaptamer receptors.

Pattern recognition has been actively exploited to develop differential sensors, or "artificial noses/tongues".[13−17] Chemists have strived to design libraries of chemically synthesized nonspecific sensing elements that respond differentially to a given molecular target. Collective responses from these libraries form a distinctive fingerprint for each target, leading to discriminative identification of a range of small organic and biological molecules.[18−28] More recently, a type of generic sensor array with green fluorescent protein and differentially functionalized gold nanoparticles has shown unprecedented ability to identify proteins selectively in a complicated matrix.[29]

It is well-known that the sensitivity and discrimination ability of a differential sensor are critically dependent on the number of sensing elements. For example, a dog's ultrasensitive smelling ability (a millionfold better than a human's) benefits from the presence of 4 billion olfactory receptor cells.[30] However, the use of large-scale sensor arrays in artificial noses/tongues is hampered by the difficulty of the molecular design and chemical synthesis of recognition elements. DNA molecules are particularly suitable for this purpose. While DNA consists of only four bases (A, T, G, and C), even a short oligonucleotide sequence (e.g., 20 bases) possesses up to billions of combinations.[31] Moreover, DNA of almost any sequence can readily be chemically synthesized and fluorescently labeled with low cost, high purity, and robust stability. Exploitation of these properties has proven successful for in vitro aptamer selection.[2] Inspired by that, we postulated that a set of designed DNA sequences may provide high structural diversity that could be used to map subtle biomolecular interactions and identify closely resembling targets.

An ideal fluorescent assay platform requires low background emission and high response reproducibility. The combination of NGO with DNA elements plays a unique role in this regard.[10,12] Graphene is an emerging one-atom-thick two-dimensional (2D) nanomaterial that has generated great interest in various areas because of its extraordinary electronic, thermal, and mechanical properties.[32,33] Very recently, biological applications of its water-soluble derivative, NGO, have been explored in the development of biosensors, drug carriers,

and antibacterial materials.[10,34,35] Importantly, NGO is a superquencher that can quench the fluorescence of virtually any fluorophore with ultrahigh efficiency,[10] which is particularly useful for background suppression in fluorescence assays. In addition, our previous molecular dynamics studies[10] revealed that single-stranded DNA (ssDNA) interacts with NGO predominantly through π stacking between DNA bases and hexagonal cells of NGO. Consequently, the interactions between DNA and NGO are relatively simple and potentially tunable with variation of the DNA length, sequence, and secondary structure.[36]

■ EXPERIMENTAL SECTION

All of the oligonucleotides were synthesized and purified by TaKaRa Inc. (Dalian, China). 6-Carboxyfluorescein (6-FAM) was labeled at the 5′ end. Graphite powder was purchased from China National Pharmaceutical Group (Shanghai, China). Subtilisin A (SubA, from *Bacillus licheniformis*), fibrinogen (Fib, from human plasma), human serum albumin (HSA), and cytochrome *c* (CC, from horse heart) were purchased from Merck. Lysozyme (Lyso, from chicken egg), horseradish peroxidase (HRP), bovine serum albumin (BSA), lipase (from *Chromobacterium viscosum*), casein (from bovine milk), and hemoglobin (Hb, from bovine blood) were purchased from Sigma-Aldrich. NGO was synthesized from graphite powder using Hummer's method.[37] The thickness of a fully exfoliated NGO sheet was ∼0.8 nm, as determined by atomic force microscopy (AFM) (Figure S1 in the Supporting Information).

In the fluorescence titration study, fluorescence spectra were collected with a Hitachi F-4500 spectrophotometer equipped with a xenon lamp excitation source. During the titration, the initial emission spectrum was recorded for DNA elements (50 nM) with excitation at 494 nm. Aliquots of a solution of NGO (1 mg/mL) were subsequently added to the solution of DNA elements. After each addition, a fluorescence spectrum was recorded. Nonlinear least-squares curve-fitting analysis was conducted to estimate the complex stability as well as the DNA effective footprint using a calculation model in which NGO was assumed to possess independent binding sites with DNA bases.

For construction of the ENSaptamer protein sensor array, DNA elements (P1−P7) and NGO were diluted with phosphate-buffered saline (PBS). The final concentrations of DNA elements and NGO were 50 nM and 10 μg/mL, respectively. After 30 min of incubation, the solutions (200 μL in each well) were loaded into a black Microlon 96-well plate (Greiner Bio-One, Germany). The fluorescence intensity at 535 nm was recorded at an excitation wavelength of 485 nm on a Tecan GENios Pro plate reader at 25 °C. Subsequently, 5 μL of protein stock solution (200 μM) was added to each well (final concentration 5 μM). After incubation for 30 min, the fluorescence intensity at 535 nm was recorded again. The difference between the readings before and after addition of protein was used as the fluorescence response (Table S2 in the Supporting Information). The nine protein targets were tested against ENSaptamer-5, ENSaptamer-6, and ENSaptamer-7 six times. The raw data matrix was processed using classical linear discriminant analysis (LDA) in SYSTAT (version 12.0). Similar procedures were also performed to identify analytical samples (various concentrations of protein, mixtures of protein, thermally denatured proteins, cells, and bacteria). In the case of serum studies, the concentrations of NGO and the DNA elements of the ENSaptamers were 100 μg/mL and 500 nM, respectively.

In the case of the cell-sensing assay, cells were grown in Gibco RPMI-1640 cell culture medium, spun down, resuspended in RPMI-1640 medium (without serum protein/antibiotics), and counted using a hemocytometer. The cell suspension was reacted with ENSaptamer-7 for 30 min (final concentation of 5000 cells in 200 μL). The change in fluorescence intensity was used as the output response.

For bacteria identification, bacteria were separated from the growth medium and resuspended in PBS to achieve an optical density (OD) of 1.0 at 600 nm. The bacteria solution was added to each sensor element (ENSaptamer-7) up to a final concentration with an OD of 0.05. The change in fluorescence intensity was used as the output response.

In the case of testing of unknown protein samples, 46 samples were tested with the same procedures as for the training samples, and the resulting fluorescence response patterns were subjected to LDA. The samples were ranked in terms of their Mahalonobis distances to the groups generated through the training matrix (Table S3 in the Supporting Information) and returned the nearest samples to the respective groups (Table S5 in the Supporting Information). Similar procedures were also performed to test unknown cell and bacteria samples.

■ RESULTS AND DISCUSSION

To interrogate the DNA−NGO interactions experimentally, we designed a series of 20-base ssDNA probes (P1−P7) tagged with the fluorescent dye, 6-FAM. The choice of these sequences reflects sequence and structural diversity. Fluorescent titrations of these probes was performed in the presence of NGO. We found that their fluorescence was all quenched by NGO (Figure 1), with the two structured probes P6 (G-
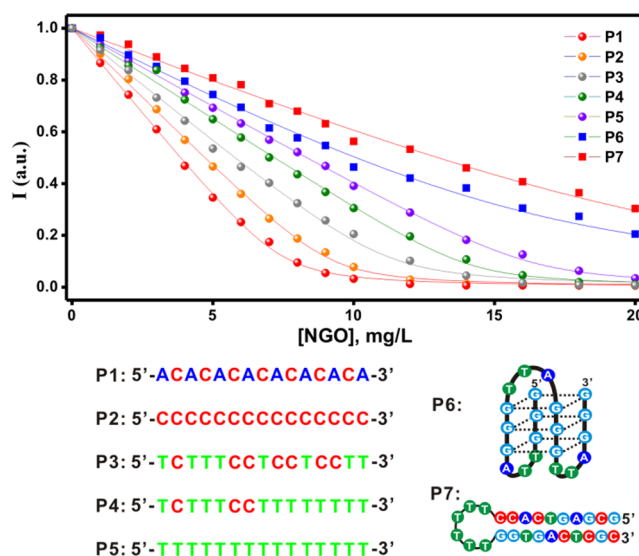
Figure 1. Fluorescence titrations of fluorescently labeled ENSaptamers P1−P7 with NGO. The concentration of each DNA probe was 50 nM. The intensity of fluorescence was normalized and plotted against the mass concentration of NGO. The sequences and structures of the ENSaptamers are shown at the bottom.

quadraplex) and P7 (hairpin) being least perturbed. The quenching states of the linear probes P1−P5 were sensitively dependent on the base combination. Nonlinear least-squares curve-fitting analysis[38] of each quenching curve (see the Supporting Information) led to two key parameters, the binding free energy ($-\Delta G$) and the effective DNA footprint (β), that provide a quantitative measure of these interactions (Table 1). The unstructured ssDNA probes P1−P5 possessed comparable binding energies with NGO ($-\Delta G = 52.7 \pm 0.9$ kJ/mol). These values were nevertheless much higher than those for the structured DNA probes P6 and P7 ($-\Delta G = 47.7 \pm 0.3$ kJ/mol).

The effective DNA footprint, β, is defined as the average area of NGO occupied by an individual DNA strand, which sensitively reflects the microscopic binding state of the DNA probe on NGO. As a general trend, the β values for P1−P5 increased when A was replaced with C and when C was

Table 1. Experimentally Determined Values of the DNA–NGO Microscopic Binding Constants (K_s), Binding Free Energies ($-\Delta G$), and Effective DNA Footprints (β)

DNA	K_s (10^8 M^{-1})	$-\Delta G$ (kJ/mol)	β (nm^2)
P1	12.0	51.8	326
P2	15.8	52.5	401
P3	13.1	52.0	490
P4	24.9	53.6	617
P5	20.1	53.1	714
P6	2.0	47.4	735
P7	2.6	48.0	980

Table 2. ENSaptamer Compositions

ENSaptamer	composition
ENSaptamer-5	P1, P2, P5, P6, P7
ENSaptamer-6	P1, P2, P4, P5, P6, P7
ENSaptamer-7	P1, P2, P3, P4, P5, P6, P7

replaced with T (Table 1). This trend is consistent with the previously reported binding affinities of DNA bases to NGO (A > C > T).[39] In addition, β increased as a function of the DNA length, while 20-base DNA sequences provided reasonable affinity (Table S2 in the Supporting Information and Figure 2).
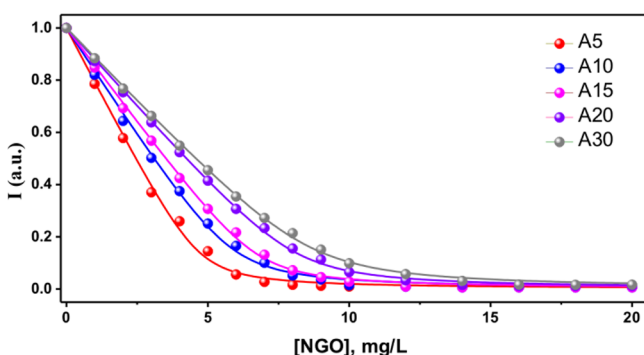
Figure 2. Fluorescence titrations of fluorescently labeled DNAs of different lengths with NGO. The concentration of each DNA was 50 nM. The fluorescence intensity was normalized and plotted against the mass concentration of NGO. The sequences and structures of the ENSaptamers are shown at the bottom of Figure 1. The DNA sequences were the following: A5, 5′-AAAAA-3′; A10, 5′-AAAAAAAAAA-3′; A15, 5′-AAAAAAAAAAAAAAA-3′; A20, 5′-AAAAAAAAAAAAAAAAAAAA-3′; A30, 5′-AAAAAAAAAAAAAAAAAAAAAAAAAAAAAA-3′.

Hence, β provides an effective tool for designing ENSaptamers possessing diverse interactions with NGO. Since structured DNA probes (e.g., P6 and P7) usually possess smaller β values than linear probes, they are particularly useful for designing ENSaptamer elements with low β values, which is beneficial for the discrimination ability of sensor arrays. Interestingly, while the size and shape variations of NGO are rather large (as shown in Figure S1 in the Supporting Information), we found the values of both $-\Delta G$ and β to be highly reproducible for each given sequence. This reflects the fact that β and the fluorescence quenching are predominantly determined by microscopic contact between DNA and the uniform 2D surface of NGO rather by the apparent lateral size distribution of NGO.

We then constructed a set of ENSaptamer elements to identify nine proteins (all at 5 μM). These elements were chosen from probes P1–P7 (Table 2) on the basis of the criterion that they have relatively evenly distributed β values. The selected proteins were SubA, Fib, Hb, CC, Lyso, HRP, BSA, lipase, and casein, which have different molecular weights, isoelectric points (pIs), and oligomeric states. Initially, these proteins were tested on the NGO–ENSaptamer sensing

platform with ENSaptamer-5, the five-element subset containing P1, P2, P5, P6, an P7. The presence of the various proteins led to differential fluorescence responses due to their interactions with NGO and the DNA probes (Figure 3a). Fluorescence enhancement was observed for most of the probes (all of the unstructured probes and some structured ones), suggesting that bound DNA strands were released into the solution as a result of the competitive displacement of proteins. Some structured probes (P6 and P7) resulted in a slight decrease in fluorescence intensity (10 out of 18), which was presumably due to perturbation of the DNA structures by the proteins that made the probes more accessible to NGO. The resultant fluorescence response patterns were quantitatively analyzed using LDA, a powerful statistical technique.[40] Six replicates were tested for each protein sample, and the raw data were subjected to LDA to generate four canonical factors (81.1, 16.4, 1.3, and 1.2% of the variation), which represent linear combinations of the fluorescence response matrix (five NGO–ENSaptamers × nine proteins × six replicates). The first two most significant discrimination factors were employed to generate a 2D plot (Figure 3b) in which each point represents the response pattern for an individual protein sample against the sensor array. Importantly, we were able to cluster the 54 canonical fluorescence response patterns (9 proteins × 6 replicates) into nine distinct groups (Figure 3b). The majority of the protein targets (six out of nine) were clearly identified in this pattern recognition using ENSaptamer-5. However, three proteins (BSA, HRP, and Fib) exhibited significant overlap between their 95% confidence ellipses (marked in the yellow square), suggesting the limited discrimination ability of ENSaptamer-5.

To improve the resolving power of this sensor array, we increased the number of DNA elements and evaluated whether the poorly resolved class (BSA, HRP, Fib) could be separated. Significantly, when six DNA elements were employed (ENSaptamer-6), BSA was effectively separated from the other two proteins (Figure 3c). The jackknifed classification matrix, which used functions computed from all of the data except the case being classified, showed that the classification accuracy was improved from 96% for ENSaptamer-5 to 100% for ENSaptamer-6 and ENSaptamer-7. It is noteworthy that individual sensor elements only had very low classification accuracy (39–70%; Figure S2 in the Supporting Information) on the basis of six replicates of the measurement. Despite the increased the classification accuracy, HRP and Fib still showed significant overlap in the 2D canonical score plot. We further added one DNA element to obtain ENSaptamer-7, which properly identified all nine proteins with different 3D structures and distinctive surface properties without significant overlap. The Euclidean distance (i.e., the length of the line segment connecting the points) between HRP and Fib increased from 2.6 to 4.7, which completely separated the two in the plot (Figure 3d). This NGO–ENSaptamer sensor array was sufficiently sensitive to identify proteins at nanomolar concentrations (Figure 4). The linearity of the dose–response curve suggests that the NGO–DNA interactions are homoge-
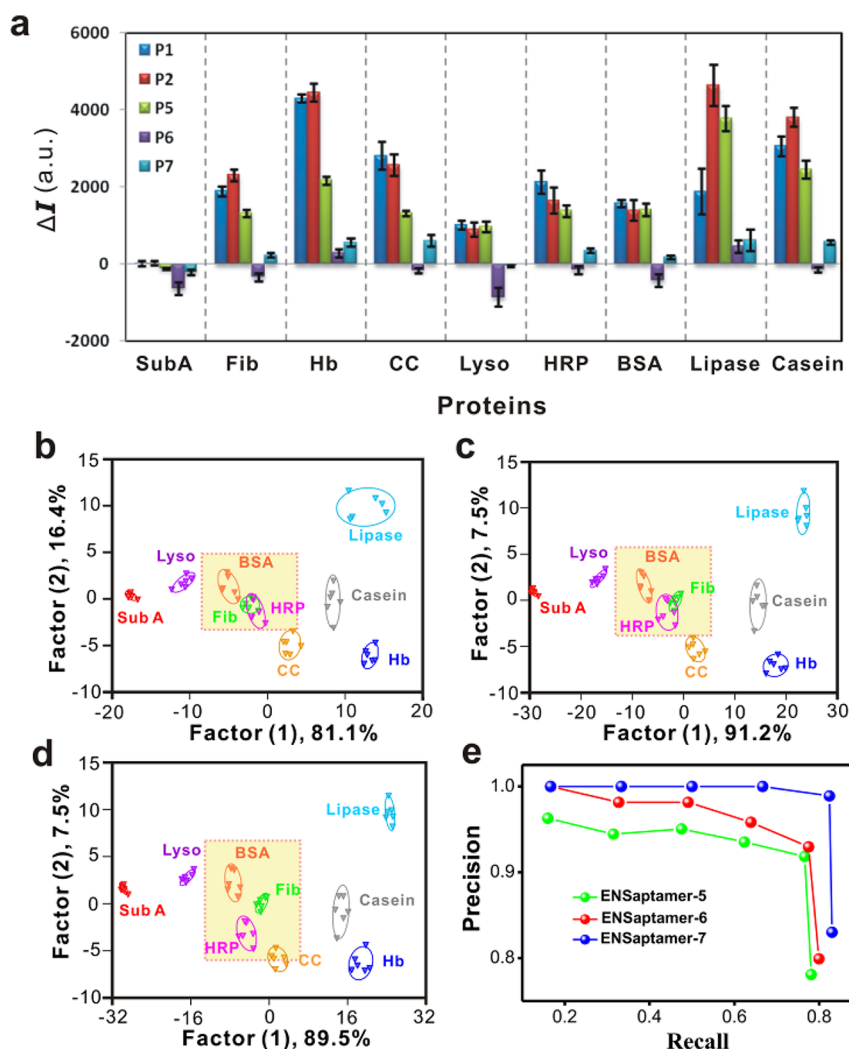
Figure 3. Protein identification with the NGO–ENSaptamer sensing platform. (a) Fluorescence response patterns of ENSaptamer-5 against various proteins (all at 5 μM): subtilisin A (SubA), fibrinogen (Fib), hemoglobin (Hb), cytochrome c (CC), lysozyme (Lyso), horseradish peroxidase (HRP), bovine serum albumin (BSA), lipase, and casein. Error bars represent standard deviations of six parallel measurements. (b) Canonical score plot for the NGO–ENSaptamer-5 sensor array containing P1, P2, P5, P6, and P7. Six of the nine proteins were properly identified, but three (BSA, Fib, and HRP) overlapped. (c) Canonical score plot for the NGO–ENSaptamer-6 sensor array containing P1, P2, P4, P5, P6, and P7. BSA was separated from Fib and HRP in this plot. (d) Canonical score plot for the NGO–ENSaptamer-7 sensor array containing P1–P7. All nine proteins were well-separated and properly identified. (e) Precision–recall curves for the NGO–ENSaptamer sensor arrays. ENSaptamer-7 showed high precision (>99%) at high recalls (<83%).

neous and stable and that the sensor array is highly reproducible. In addition, we showed that ENSaptmers were extremely sensitive to the protein conformation. When the proteins were thermally denatured, the difference became negligible, and the data were clustered in a specific region of the canonical score plot regardless of their molecular weights and original pIs (Figure 5). This suggests that the 3D structure and distinct surface characteristics of proteins form the basis for differential sensing with ENSaptamers.

The performance of the ENSaptamers was further evaluated with precision–recall (PR) curves (Table S1 in the Supporting Information), which use the precision (the proportion of the retrieved categories that are relevant) and the recall (the proportion of the total number of relevant categories that have been retrieved) as the two primary factors.[41] The retrieved proteins were ranked by the Euclidean distance of the query protein and returned the k nearest samples. Clearly, the curve for ENSaptamer-7 was above those for ENSaptamer-5 and

ENSaptamer-6 (Figure 3e), confirming that ENSaptamer-7 led to better sensing performance in terms of both precision and recall. We note that ENSaptamer-7 achieved very high precision (99%) even at high recall (83%).

The robustness of the ENSaptamer-based protein sensing arrays was tested using a list of unknown protein samples generated from nine kinds of proteins. The unknown samples were ranked in terms of Mahalonobis distance to the groups generated through the training matrix (Table S3 in the Supporting Information) and returned the nearest samples to the respective groups. In our studies, only three samples were incorrectly identified, which indicates a 93.5% accuracy for the 46 unknown samples (Table S5 in the Supporting Information).

The protein recognition ability of ENSaptamers was not sacrificed in mixtures. We tested mixtures of Hb and Lyso with different molar ratios (Hb/Lyso = 10/90, 30/70, and 50/50 with 10 μM total protein). These mixtures, as well as pure Lyso
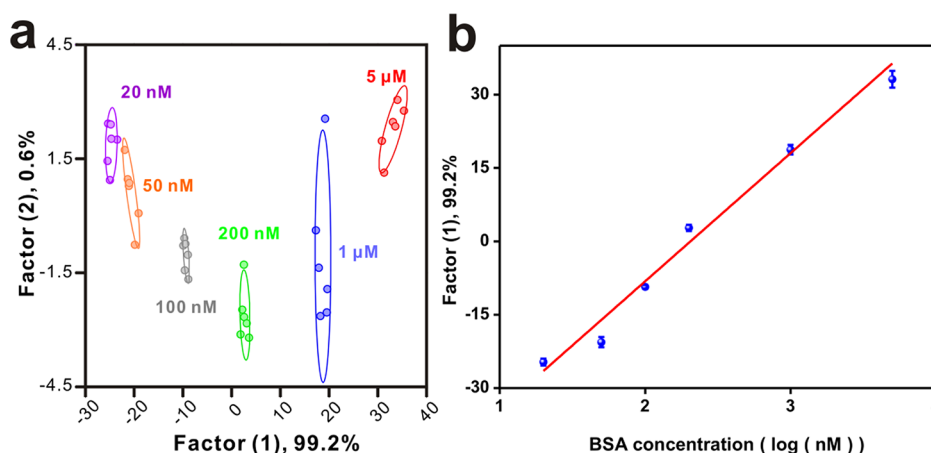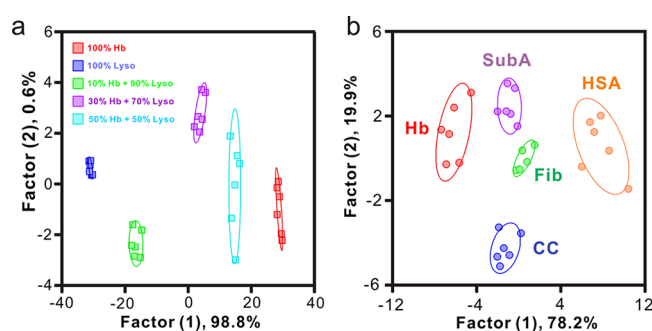
Figure 4. Identification of proteins at various concentrations using the ENSaptamer-7 sensor array. (a) Canonical score plot for fluorescence response patterns obtained with ENSaptamer-7 against different concentrations of BSA (20 nM, 50 nM, 200 nM, 1 μM, and 5 μM). Notably, since factor (2) was smaller than 1%, it was possible simply to use factor (1) to identify the protein. The 2D plot was still employed for consistency with other plots. (b) Plot of the first discriminant factor vs the logarithm of the BSA concentration.
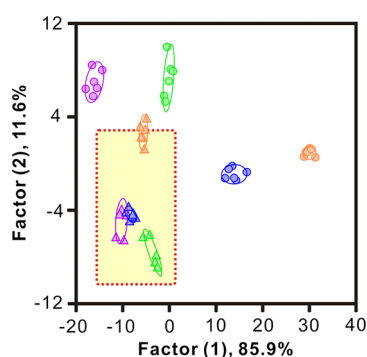
Figure 5. Canonical score plot using the first two factors of the simplified fluorescence response patterns obtained with ENSaptamer-7 against native proteins (circles) and thermally denatured proteins (triangles). Colors represent different proteins: purple, SubA; blue, Fib; green, Lyso; orange, HSA.

Figure 6. Protein identification in mixtures and serum. (a) Canonical score plot for ENSaptamer-7 against protein mixtures. Left to right: pure Lyso; 10% Hb + 90% Lyso; 30% Hb + 70% Lyso; 50% Hb + 50% Lyso; pure Hb. In each case, the total protein concentration was 10 μM. Notably, since factor (2) was smaller than 1%, it was possible simply to use factor (1) to identify the protein. The 2D plot was still employed for consistency with the other plots. (b) Canonical score plot for ENSaptamer-7 against proteins spiked in human serum. Five proteins (SubA, Fib, Hb, CC, and HSA, each at 5 μM) were properly identified.

and Hb, were clearly distinguished from each other in the LDA plot and properly arranged with the order of ratios in the dimension of the first factor (Figure 6a). As a further test, proteins (all at 5 μM) were spiked in human serum, a complex matrix with high overall protein content (∼1 mM, 71 mg mL^{-1}), and analyzed with the NGO−ENSaptamer-7 sensing array. Because of the presence of the high-OD background of human serum, higher concentrations of the DNA probes (500 nM) and NGO (100 μg mL^{-1}) were employed to obtain reliable responses. Under these conditions, high sensing reproducibility was retained, and we obtained precise identification of 5 proteins with 100% identification accuracy and essentially no overlap in the canonical score plot (Figure 6b).

ENSaptamers also provide a versatile platform for the detection of cells and microorganisms, which is important for diagnosis of cancers and bacterial infections. As a proof of concept, five different normal and cancerous cell lines were tested, and the resultant fluorescence responses were analyzed with LDA. With the NGO−ENSaptamer-7 sensor array, three types of human cancer cells [HeLa (cervical), 786-O (kidney), and SH-SY5Y (brain)] and one type of mouse cancerous cell line (RAW 264.7) were well-separated from each other as well as from the human normal cell line (CCRF-CEM) (Figure 7a).

An accuracy of 90% (18 out of 20) was observed in the test of 20 unknown cell samples (Table S11 in the Supporting Information). Similarly, ENSaptamer-7 could discriminatively identify six strains of bacteria from three different species (*Escherichia coli*, *Shigella*, and *Salmonella*) (Figure 7b). We observed an accuracy of 86.7% (26 out of 30) in the case of an unknown sample test (Table S14 in the Supporting Information).

Nucleic acid aptamers are an elegant example of the exploitation of recognition abilities of nucleic acids (aside from their genetic roles). Nevertheless, the technical difficulty and cost of selecting high-affinity aptamers remain as major barricades for diagnostic and therapeutic applications of aptamers. ENSaptamers provide a conceptually new alternative that does not rely on authentic high-affinity receptors. While individual "nonspecific" DNA elements do not possess sufficient specificity for the given target, their ensemble collectively "smells" out the target like a "nose" with high precision on the basis of differential interactions between each element and the target, which may include versatile molecular

13847

dx.doi.org/10.1021/ja305814u | *J. Am. Chem. Soc.* 2012, 134, 13843−13849
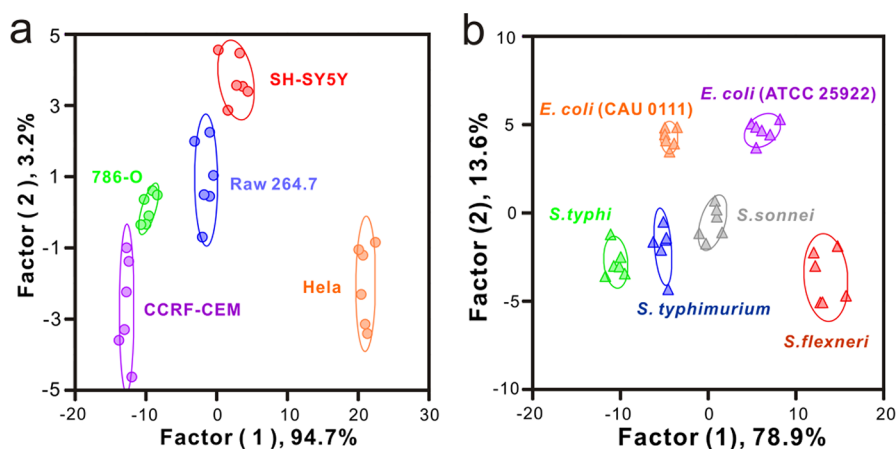
Figure 7. Identification of cells and bacteria with the NGO−ENSaptamer-7 sensing platform. (a) Canonical score plot for ENSaptamer-7 against normal and cancerous cell lines (5000 cells in 200 μL). Three types of human cancer cells [HeLa (cervical), 786-O (kidney), and SH-SY5Y (brain)], a mouse cancerous cell line (RAW 264.7), and a human normal cell line (CCRF-CEM) showed well-separated patterns. (b) Canonical score plot for ENSaptamer-7 for bacteria with different species and strains (0.05 OD in 200 μL). Three species of microorganisms (*Escherichia coli*, *Shigella*, and *Salmonella*) were employed, each containing two strains of bacteria: *E. coli* CAU 0111, *E. coli* ATCC 25922, *Shigella sonnei*, *Shigella flexneri*, *Salmonella typhi*, and *Salmonella typhimurium*.

interactions such as electrostatic attraction/repulsion, hydrophobic interactions, and possibly hydrogen bonding. Also importantly, ENSaptamers are highly adaptive, similar to natural olfactory and gustatory systems. Since the discrimination ability is easily expandable with the addition of a new DNA element with a distinctive β value, any given target could in principle be discriminatively identified from closely resembling species using an ENSaptmer with a sufficiently large library. Alternatively, it is also possible to perform fault-tolerant analysis to cluster proteins with similar properties by reducing the number of DNA elements.

CONCLUSION

The combination of ENSaptamers and NGO brings about several unprecedented advantages. First, the number of DNA elements is almost unlimited, since DNA strands of different sequences, structures, and lengths interact differentially with the given target. We have also proven that a library can be made sufficiently large to identify unknown proteins with appropriate training. Second, NGO provides large, flat, and relatively homogeneous surfaces that can adsorb DNA with high reproducibility. Hence, it is convenient to design DNA elements with simple knowledge of the binding affinity of DNA bases to NGO and structural information of DNA sequences. The experimentally determined β value provides a guideline for such selection. Third, the superquenching ability of NGO ensures high detection sensitivity with low background noise. Therefore, we expect this NGO−ENSaptamer sensing platform to hold great promise for biomedical diagnostics, and the concept of ENSaptamers might be extended to other affinity-receptor-based applications, including bioimaging and therapeutics.

ASSOCIATED CONTENT

Ⓢ Supporting Information

Notes on AFM characterization of NGO, titrations of proteins with ENSaptamers, estimation of the binding constants and precision−recall values; raw data from all of the sensing experiments using ENSaptamers. This material is available free of charge via the Internet at http://pubs.acs.org.

AUTHOR INFORMATION

Corresponding Author

hujun@sinap.ac.cn; fchh@sinap.ac.cn

Notes

The authors declare no competing financial interest.

ACKNOWLEDGMENTS

REFERENCES

(1) Ellington, A. D.; Szostak, J. W. *Nature* **1990**, *346*, 818−822.
(2) Hermann, T.; Patel, D. J. *Science* **2000**, *287*, 820−825.
(3) Nimjee, S. M.; Rusconi, C. P.; Sullenger, B. A. *Annu. Rev. Med.* **2005**, *56*, 555−583.
(4) Willner, I.; Zayats, M. *Angew. Chem., Int. Ed.* **2007**, *46*, 6408−6418.
(5) Liu, J. W.; Cao, Z. H.; Lu, Y. *Chem. Rev.* **2009**, *109*, 1948−1998.
(6) Paige, J. S.; Wu, K. Y.; Jaffrey, S. R. *Science* **2011**, *333*, 642−646.
(7) Mitchell, P. *Nat. Biotechnol.* **2002**, *20*, 225−229.
(8) Patterson, S. D.; Aebersold, R. H. *Nat. Genet.* **2003**, *33*, 311−323.
(9) Lancet, D.; Benarie, N. *Curr. Biol.* **1993**, *3*, 668−674.
(10) He, S. J.; Song, B.; Li, D.; Zhu, C. F.; Qi, W. P.; Wen, Y. Q.; Wang, L. H.; Song, S. P.; Fang, H. P.; Fan, C. H. *Adv. Funct. Mater.* **2010**, *20*, 453−459.
(11) Balapanuru, J.; Yang, J. X.; Xiao, S.; Bao, Q. L.; Jahan, M.; Polavarapu, L.; Wei, J.; Xu, Q. H.; Loh, K. P. *Angew. Chem., Int. Ed.* **2010**, *49*, 6549−6553.
(12) Loh, K. P.; Bao, Q. L.; Eda, G.; Chhowalla, M. *Nat. Chem.* **2010**, *2*, 1015−1024.
(13) Rakow, N. A.; Suslick, K. S. *Nature* **2000**, *406*, 710−713.
(14) Albert, K. J.; Lewis, N. S.; Schauer, C. L.; Sotzing, G. A.; Stitzel, S. E.; Vaid, T. P.; Walt, D. R. *Chem. Rev.* **2000**, *100*, 2595−2626.
(15) Wright, A. T.; Anslyn, E. V. *Chem. Soc. Rev.* **2006**, *35*, 14−28.
(16) Lavigne, J. J.; Anslyn, E. V. *Angew. Chem., Int. Ed.* **2001**, *40*, 3119−3130.
(17) Bunz, U. H. F.; Rotello, V. M. *Angew. Chem., Int. Ed.* **2010**, *49*, 3268−3279.

(18) Lee, J. W.; Lee, J. S.; Chang, Y. T. *Angew. Chem., Int. Ed.* **2006**, *45*, 6485−6487.

(19) Lee, J. W.; Lee, J. S.; Kang, M.; Su, A. I.; Chang, Y. T. *Chem.— Eur. J.* **2006**, *12*, 5691−5696.

(20) Greene, N. T.; Shimizu, K. D. *J. Am. Chem. Soc.* **2005**, *127*, 5695−5696.

(21) Folmer-Andersen, J. F.; Kitamura, M.; Anslyn, E. V. *J. Am. Chem. Soc.* **2006**, *128*, 5652−5653.

(22) Buryak, A.; Severin, K. *J. Am. Chem. Soc.* **2005**, *127*, 3700−3701.

(23) Li, H. P.; Bazan, G. C. *Adv. Mater.* **2009**, *21*, 964−967.

(24) Baldini, L.; Wilson, A. J.; Hong, J.; Hamilton, A. D. *J. Am. Chem. Soc.* **2004**, *126*, 5656−5657.

(25) Zhou, H. C.; Baldini, L.; Hong, J.; Wilson, A. J.; Hamilton, A. D. *J. Am. Chem. Soc.* **2006**, *128*, 2421−2425.

(26) You, C. C.; Miranda, O. R.; Gider, B.; Ghosh, P. S.; Kim, I. B.; Erdogan, B.; Krovi, S. A.; Bunz, U. H. F.; Rotello, V. M. *Nat. Nanotechnol.* **2007**, *2*, 318−323.

(27) Green, E.; Olah, M. J.; Abramova, T.; Williams, L. R.; Stefanovic, D.; Worgall, T.; Stojanovic, M. N. *J. Am. Chem. Soc.* **2006**, *128*, 15278−15282.

(28) Wright, A. T.; Griffin, M. J.; Zhong, Z. L.; McCleskey, S. C.; Anslyn, E. V.; McDevitt, J. T. *Angew. Chem., Int. Ed.* **2005**, *44*, 6375−6378.

(29) De, M.; Rana, S.; Akpinar, H.; Miranda, O. R.; Arvizo, R. R.; Bunz, U. H. F.; Rotello, V. M. *Nat. Chem.* **2009**, *1*, 461−465.

(30) Sherwood, L. *Human Physiology: From Cells to Systems*, 7th ed.; Brooks/Cole: Belmont, CA, 2010; Chapter 6, p. 232.

(31) Clelland, C. T.; Risca, V.; Bancroft, C. *Nature* **1999**, *399*, 533−534.

(32) Novoselov, K. S.; Geim, A. K.; Morozov, S. V.; Jiang, D.; Zhang, Y.; Dubonos, S. V.; Grigorieva, I. V.; Firsov, A. A. *Science* **2004**, *306*, 666−669.

(33) Li, D.; Kaner, R. B. *Science* **2008**, *320*, 1170−1171.

(34) Liu, Z.; Robinson, J. T.; Sun, X. M.; Dai, H. J. *J. Am. Chem. Soc.* **2008**, *130*, 10876−10877.

(35) Hu, W. B.; Peng, C.; Luo, W. J.; Lv, M.; Li, X. M.; Li, D.; Huang, Q.; Fan, C. H. *ACS Nano* **2010**, *4*, 4317−4323.

(36) Li, D.; Song, S. P.; Fan, C. H. *Acc. Chem. Res.* **2010**, *43*, 631−641.

(37) Hummers, W. S.; Offeman, R. E. *J. Am. Chem. Soc.* **1958**, *80*, 1339−1339.

(38) You, C. C.; De, M.; Han, G.; Rotello, V. M. *J. Am. Chem. Soc.* **2005**, *127*, 12873−12881.

(39) Varghese, N.; Mogera, U.; Govindaraj, A.; Das, A.; Maiti, P. K.; Sood, A. K.; Rao, C. N. R. *ChemPhysChem* **2009**, *10*, 206−210.

(40) Jurs, P. C.; Bakken, G. A.; McClelland, H. E. *Chem. Rev.* **2000**, *100*, 2649−2678.

(41) Manning, C. D.; Schütze, H. *Foundations of Statistical Natural Language Processing*; MIT Press: Cambridge, MA, 1999.